



Contents lists available at ScienceDirect

Geotextiles and Geomembranes

journal homepage: www.elsevier.com/locate/geotexmem

Regular Paper

Creep rupture behaviour of elastomeric bituminous geomembrane seams

Jiying Fan^a, R. Kerry Rowe^{b,*}^a GeoEngineering Centre at Queen's-RMC, Dept. of Civil Engineering, Queen's Univ., Kingston, ON, Canada, K7L 3N6^b Barrington Batchelor Distinguished University Professor, Canada Research Chair in Geotechnical and Geoenvironmental Engineering, GeoEngineering Centre at Queen's-RMC, Dept. of Civil Engineering, Queen's Univ., Kingston, ON, Canada, K7L 3N6

ARTICLE INFO

Keywords:

Geosynthetics
 Bituminous geomembrane
 Seams
 Tensile strength
 Creep rupture

ABSTRACT

The short-term and long-term performance of bituminous geomembrane (BGM) seams are examined using both small-scale and large-scale tests. Different BGM products, different sustained tensile loads, different weld qualities, and different overburden stresses are examined. The BGM seams are shown to be very susceptible to creep rupture under sustained tensile loads. Time to rupture and strain at rupture for acceptable welds are both exponentially correlated with the sustained load, for the different BGM products examined. With the increasing tensile load from 5%, 10%, 20%, 30%, 40% of sheet maximum tensile strength, the time to rupture decreased from 30–50 days (5%), 5 days (10%), 0.8 day (20%), 0.2 day (30%), to 0.03 day (40%) and, the strain at rupture increased from 5%, 7%, 13%, 17%, to 20–30%. In large-scale tests simulating field conditions, the BGM seam creep ruptured within 24 days when the overburden stress was 20 kPa, and within ≤ 0.2 day when the overburden stress reached 50 kPa. The consequences of liquids or gases readily permeating through failed seam should be evaluated before using BGMs in an environment where tensile stresses can develop (e.g. due to differential settlement, subgrade irregularity, or downdrag).

1. Introduction

The past few decades have witnessed a substantial increase in the use of geomembranes (GMBs) for fluid containment, be they liquids or gases, and protecting the environment. Applications include modern landfills, lagoons for contaminated fluid, dams, drinking water reservoirs, tailings storage facilities, heap leach pads, etc. where escape of fluid to the surrounding environment must be minimized (Giroud and Bonaparte 1989a, 1989b; Giroud 2005; Rowe 1998, 2005, 2012, 2020; Rowe et al., 2013; Rowe and Jefferis 2022; Rowe and Fan 2022, 2024; Fan and Rowe 2022a, 2023a; Ewais et al., 2014; Pu et al., 2018; Zhan et al., 2018; Rowe and Yu, 2019; Touze 2020; Yan et al., 2021; Chang et al., 2021; Ng et al., 2023). Geomembranes may also be used as a cover liner in modern landfill and mining applications to prevent the infiltration of water and air into the waste (Rowe and Hosney 2013). Most of these facilities are lined with polymeric geomembranes such as linear low-density polyethylene, high-density polyethylene, and polyvinyl chloride (Rowe et al., 2004, 2013; Scheirs 2009). However, over the last ten years, bituminous geomembranes (BGMs) have rapidly gained momentum, particularly in mining applications.

BGMs are typically comprised of a reinforcing geotextile to provide

mechanical strength impregnated with an elastomeric bitumen and have been propagated as a strong alternative liner material due to their low permeability, high puncture resistance, low coefficient of thermal expansion, extreme temperature tolerance, steep slope capability, and high wind resistance (Peggs 2008; Touze-Foltz and Farcas, 2017; Samea and Abdelaal 2023). BGMs are multilayer composite materials that consist of a nonwoven polyester geotextile (GTX) and a glass fleece sheet as the reinforcement core which is coated with bitumen to create a flexible and impermeable sheet (Peggs 2008; Samea and Abdelaal 2023). The bitumen used in BGMs is typically modified using elastomers such as styrene-butadienestyrene (SBS) to reduce its temperature sensitivity (Scheirs 2009; Touze-Foltz and Farcas, 2017). The top surface of the BGM is commonly sanded to increase the interface friction strength while the bottom surface is bonded to a polyester film to prevent the self-adhesion of the BGM roll during storage.

Seaming (welding) is one of the key elements affecting the integrity of the liner in the field. Rollin et al. (1999) reported that 55% of the defects in exposed geomembranes occurred at seams. Problems in the field often originate at seams (Peggs et al., 2014; Rowe and Shoaib 2017; Zhang et al., 2017) because they are locations where: (a) there is local stress magnification due to the eccentricity of loading which increases

* Corresponding author.

E-mail addresses: jiying.fan@queensu.ca (J. Fan), kerry.rowe@queensu.ca (R.K. Rowe).<https://doi.org/10.1016/j.geotexmem.2024.07.003>

Received 23 May 2024; Received in revised form 6 July 2024; Accepted 9 July 2024

Available online 4 August 2024

0266-1144/© 2024 Elsevier Ltd. All rights are reserved, including those for text and data mining, AI training, and similar technologies.

with material thickness (Giroud et al., 1995; Kavazanjian et al., 2017) and (b) heat and pressure are applied in an attempt to fuse the two panels. Although, like polymeric geomembranes, where seaming requires specialized thermal welding equipment and training, BGMs are often promoted as being relatively easy requiring only a propane torch and a roller, which can be undertaken by local labour thus allowing for faster and cheaper installation (Peggs 2008; Scheirs 2009).

The creep behaviour of the viscoelastic bitumen in a BGM is affected by applied stress, temperature, bitumen and elastomer characteristics and content. Francey and Rowe (2024) conducted tests to investigate the impact of thickness reduction and squeeze-out on the tensile performance of BGM seams and concluded that to increase the failure time of BGM seam under a sustained tensile load, there should be a thickness reduction of ~0.4 mm and ≥6 mm squeeze out bead. Francey and Rowe (2024) examined a BGM with a nominal thickness of 4 mm subjected to sustained tensile load between 4 kN/m and 12 kN/m and demonstrated that seams that meet typical short-term strength requirements can readily creep to failure. Tensions can be induced in seams in many ways including one or more of the following: by subgrade imperfections (Tang et al., 2021; Cheng et al., 2020), differential settlement, water pressure, etc. (e.g., Addis et al., 2016).

Addis et al. (2016) reported numerous BGM seam failures in the field thereby identifying an issue with the time-dependent failure of BGM seams. Francey and Rowe (2024) showed there was an issue with the time-dependent failure of BGM seams over a small range of stresses when the seam was subject to uniaxial tension (shear) for a different BGM product from that used by Addis et al. (2016). To date, no large-scale simulation on the field performance of BGM seams has been conducted. Thus, the objectives of this paper are to: (1) examine the impact of a wide range of sustained tensile loads between 1 and 10 kN/m on the time to rupture and strain at rupture for BGM seams; (2) test the difference in the performance of seams in BGM from two manufacturers; (3) explore the impact of seaming process on the weld quality and the mechanical properties of the weld; and (4) investigate the creep rupture of BGM seams under simulated field conditions in a large-scale tests apparatus.

2. Experimental investigation

2.1. Materials

This study examines two BGMs (denoted as BGM1 and BGM2; see Table 1) from different manufacturers. Both BGMs were made of elastomeric bitumen to reduce the temperature sensitivity, and both had a sanded upper surface and a smooth underside coated with a polyester (PE) film. BGM1 with a nominal thickness of 4.1 mm and mass per unit area of 4700 g/m² included a composite nonwoven polyester geotextile (GTX) and glass fleece layer. BGM2 with a nominal thickness of 3.2 mm

Table 1
Initial properties of the materials examined (mean ± standard deviation).

Property	BGM1	BGM2
Nominal thickness (mm)	4.1	3.2
Glass fleece Reinforcement (g/m ²)	50 ^a	\
Nonwoven geotextile reinforcement (g/m ²)	235 ^a	200 ^a
Mass per unit area (g/m ²)	4700 ^a	4300 ^a
Machine direction maximum tensile strength σ_M (kN/m)	29.0 ± 0.9 ^{b,c}	21.0 ± 1.4 ^b
Machine direction elongation at σ_M (mm)	44 ± 0.2 ^{b,c}	47 ± 3.6 ^b
Cross-machine maximum tensile strength σ_M (kN/m)	21.8 ± 0.3 ^{b,c}	19.5 ± 2 ^b
Cross-machine elongation at σ_M (mm)	47 ± 2.1 ^{b,c}	48 ± 4.5 ^b

Notes.

^a Values from manufacturer datasheet.

^b 10 replicates were examined for each property.

^c Data provided by Samea and Abdelaal (2023).

and mass per unit area of 4300 g/m² included a single nonwoven polyester GTX core. The maximum tensile strength (MTS) in the machine and cross-machine direction was 29.0 ± 0.9 kN/m and 21.8 ± 0.3 kN/m, respectively, for BGM1 and 21.0 ± 1.4 kN/m and 19.5 ± 2 kN/m, for BGM2 (Table 1 and Fig. 1a). The cross-machine direction was considered to be the most relevant direction for investigating the shear and tensile properties of BGM seams since the largest length of BGM seamed panels is generally oriented parallel to the machine direction, leaving the shear and tensile loading predominately engaged along the cross-machine direction. Thus, unless otherwise noted, the sheet was tested along the cross-machine direction.

2.2. Field seaming

The field torch seaming was conducted outdoors at ~18 °C ambient temperature on a smooth concrete pavement. The overlap of the top panel and bottom panel in the machine direction was 200 mm. The PE film along the underside top panel edge was removed before the 200-mm-width overlapped section was heated by a single nozzle propane torch. Pressure was applied to the overlap immediately after heating using a 10 kg steel roller. The squeeze-out of the melted bitumen at the edge of the weld was 0 mm for all the seamed BGM2 panels, while the squeeze-out of the seamed BGM1 panels was predominately 0 mm with one exception of 3 mm. The seamed specimens were left in situ to cool for approximately 1 h before being transported to laboratory for storage at 21 ± 2 °C. After more than 24 h acclimatization to lab conditions, specimens were cut using a stainless-steel blade for testing.

2.3. Tensile shear strength testing

Tensile shear strength testing was conducted based on ASTM D7056 to evaluate the quality of BGM seams at constant room temperature of 22 °C. This was an index-type test used for quality assurance and quality control purposes. Specimens with width of 50 mm and length of 400 mm were prepared (Fig. 1b). Each specimen was secured 50 mm from either leading edge of the overlapped seam, resulting in a grip-to-grip separation 100 mm greater than the seam width. The test was performed using a constant machine crosshead speed of 50 ± 2.5 mm/min until the specimen was ruptured. After rupture, the break location was recorded as either within the seam itself or within the sheet adjacent to the seam.

2.4. Constant tensile load testing

Constant tensile load testing was conducted based on a modified ASTM D5262 procedure to evaluate the unconfined tension creep and creep rupture behavior of BGM seams at constant temperature of 22 °C when subjected to a sustained tensile loading. Specimens with width of 200 mm and length ≥400 mm were prepared (Fig. 1c). Each specimen was clamped 50 mm from either leading edge of the overlapped seam, resulting in a grip-to-grip separation 100 mm greater than the seam width. Sustained tensile loading of 10 kN/m, 8 kN/m, 6 kN/m, 4 kN/m, 2 kN/m, and 1 kN/m was applied on the specimens, corresponding to 45.9%, 36.7%, 27.5%, 18.3%, 9.2%, 4.6% of the sheet tensile strength for BGM1 and 51.4%, 41.1%, 30.8%, 20.5%, 10.3%, 5.1% for BGM2. The extension of the specimen and time until rupture during each test were recorded.

2.5. Geosynthetic liner longevity/leakage simulator testing

The large-scale geosynthetic liner longevity/leakage simulator (GLLS) testing was conducted in a rigid cylindrical steel test cell with an inside diameter of 1000 mm and height of 700 mm to evaluate the rupture time of BGM seams and leakage after rupture under the simulated field conditions at constant room temperature of 22 °C (Fig. 2). Similar tests were conducted by Rowe and Fan (2021, 2022) and Fan and Rowe (2023b, 2024a, 2024b) using a smaller test cell with an inside

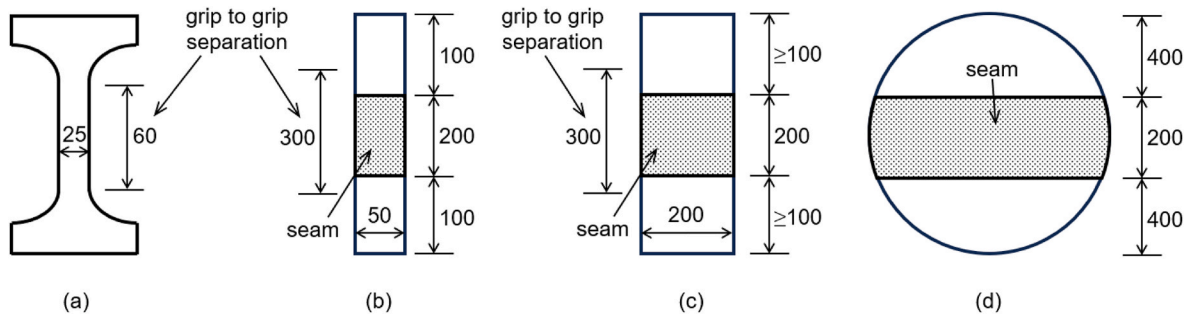


Fig. 1. Dimensions of the specimen tested for (a) tensile strength based on ASTM D7275, results given in Table 1; (b) tensile shear strength based on ASTM D7056, results given in Table 2; (c) constant tensile load testing based on ASTM D5262, results given in Table 3; (d) geosynthetic liner longevity/leakage simulator testing (GLLS, simulated field conditions), results given in Table 4. (Note: dimensions in mm).

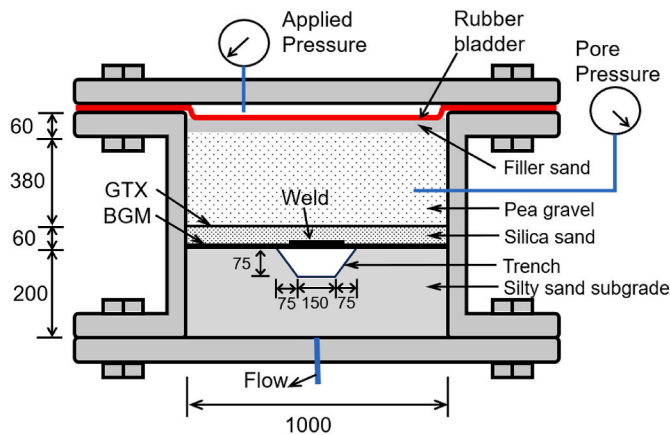


Fig. 2. Cross section through a geosynthetic liner longevity/leakage simulator (GLLS) test cell (Note: dimensions in mm).

diameter of 590 mm. A total vertical pressure was applied by introducing air pressure on top of a rubber bladder secured tightly between the lid and the body of the test cell. Pore pressure could be applied by injecting water into the cell (Fig. 2). Friction along the inner sidewall of the cell was minimized by two layers of 0.1-mm-thick polyethylene sheets, with a special lubricant between two layers allowing the outer layers to slip with very little resistance as the soil inside the cell consolidated.

The cell was filled from the bottom up as follows: geocomposite drain, silty sand subgrade with fines (<75 μm) content of ~20% ($d_{85} = 0.4$ mm, $d_{50} = 0.2$ mm, $d_{15} = 0.05$ mm; detail properties given by Fan and Rowe 2022b; 2023d) and thickness of 200 mm (Fig. 3a), central seamed BGM panel with a diameter of 1000 mm (Fig. 1d, 3b) and 60-mm-thick silica sand ($d_{85} = 1.3$ mm, $d_{50} = 1.2$ mm, $d_{15} = 1$ mm) protection layer above the BGM, GTX separation layer with mass per unit area of 450 g/m² (detail properties given by Fan and Rowe 2023c), 380-mm-thick pea gravel, and filler sand to fill the gap between pea gravel and rubber bladder (Fig. 2). There was a trench in the central silty sand subgrade surface with dimensions of 300 mm × 600 mm on top, 150 mm × 600 mm at the bottom, and depth of 75 mm (Figs. 2 and 3a). The trench was to simulate the subgrade imperfection during construction when the BGM was used as the bottom barrier, e.g., ruts arising from a scarper/truck tire or a discontinuity between passes of a smooth drum finishing roller. It could also be used to simulate the uneven or differential settlement of the underlying waste, triggered by waste degradation/consolidation or thawing of frozen waste, when the BGM was used as a cover system for waste facilities.

Test 1 had one loading stage with a constant total pressure σ_v of 20 kPa and pore pressure of 12 kPa above the BGM upper surface. Test 2 and Test 3 had three loading stages with σ_v of 30 kPa at Stage 1, 40 kPa at

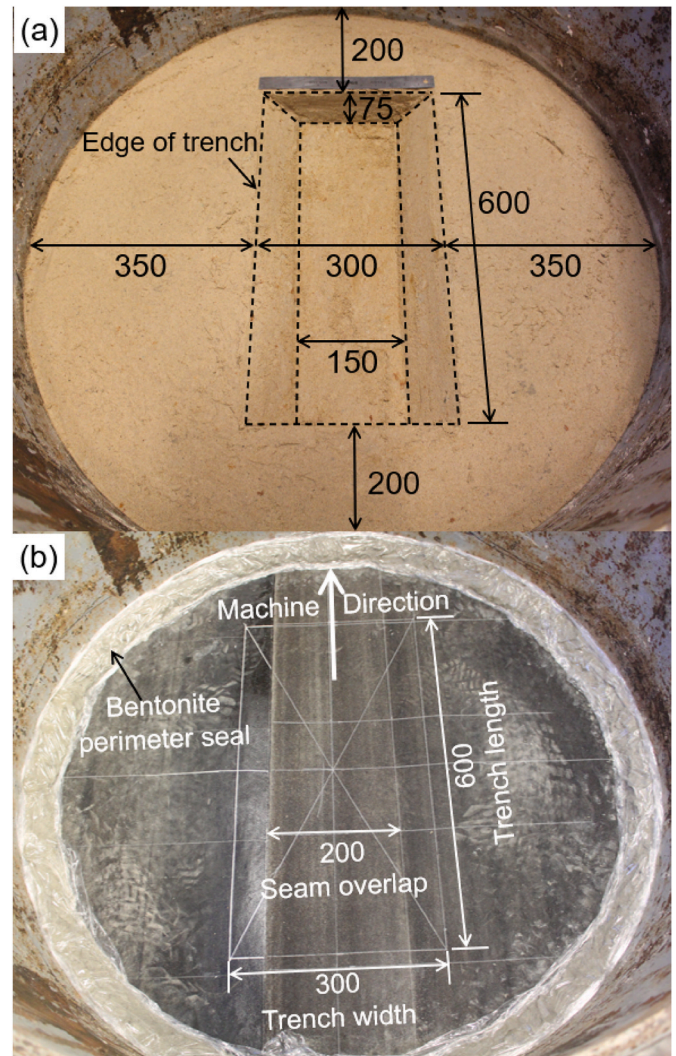


Fig. 3. GLLS test setup for (a) trench in the middle of the subgrade beneath the BGM, (b) BGM and seam positions. (Notes: dimensions in mm; the trench was to simulate the subgrade imperfection during construction, e.g., ruts arising from a scarper or truck tire or a discontinuity between passes of a smooth drum finishing roller. It could also be used to simulate the uneven or differential settlement of the underlying waste, triggered by waste degradation/consolidation or thawing of frozen waste, when the BGM was used as a cover system for waste facilities).

Stage 2, and 50 kPa at Stage 3. Pore pressure inside the cell above the BGM was ~40% of σ_v at each loading stage (i.e., 12 kPa at Stage 1, 16 kPa at Stage 2, 19 kPa at Stage 3) for Test 2 and Test 3. The loading duration at each stage for Test 2 and Test 3 was 3 days for Stage 1, 1 day for Stage 2, and ≥ 6 days for Stage 3. Rupture of BGM seam was manifested by a sudden drop in pore pressure above the BGM monitored via a pore pressure transducer and a following detection of leakage through a port located at the bottom of the GLLS cell (Fig. 2). Subsequently, leakage was collected and leakage rate was adjusted to 20 °C based on the temperature of the collected leakage.

3. Test results

3.1. Tensile shear strength testing

For the five BGM1 seamed specimens (sourced from five different seamed panels) examined at a constant room temperature of 22 °C, the peak seam strength was between 17.4 kN/m and 19.1 kN/m (Table 2). Defining the **weld factor** as the **ratio of peak seam strength to the sheet maximum tensile strength** (MTS), the weld factor for the seamed BGM1 specimens ranged from 0.80 to 0.88, all meeting the typical requirement of 0.8 weld factor as the lower limit for acceptance of BGM seam based on manufacturer guidelines. The break location was within the seam for both the largest 0.88 and smallest 0.80 weld factors, while the break location shifted to the sheet adjacent to the seam with the weld factor between 0.83 and 0.85 (Table 2). The thickness reduction of seam for BGM1 specimen, defined as the sum of the top and bottom panels thickness away from the seam minus the thickness of the seam, was generally higher when the break location was within the sheet relative to the break location within the seam. Post-failure observation of the ruptured seam showed that the geotextile within the core of top panel was not engaged with the geotextile within the bottom panel during the seaming process.

For BGM2 seamed specimens No.1 to No.7 sourced from two welded panels, the weld factors were generally ≥ 0.8 and could be classified as “acceptable weld” with one exception of 0.78 for specimen No.1 (Table 2). Contrarily, for BGM2 specimens No.8 to No.11 obtained from one seamed panel (different panel from specimens No.1 to No.7), all the welds were “unacceptable weld” with weld factors lower than 0.8. The thickness reductions were all 0.1 mm for those “acceptable weld” and were 0.2 for those “unacceptable weld”. The break locations for BGM2 specimens were all within the seam instead of within the sheet region, even though the weld factor was as high as 0.89 for No.7 specimen (Table 2). Similar to BGM1 specimens, post-failure observation of the ruptured BGM2 seam showed that no geotextile engagement arose from

the seaming process.

The aforementioned thickness reduction of BGM weld was measured by a caliper as this was regarded as an easy way of evaluating the quality of BGM seams in the field. Based on the results in Table 2, this parameter basically did not give a good indication of weld factor for both BGM1 and BGM2 welds examined if no geotextile was engaged in the seam. For example, the largest weld factor of 0.88 for BGM1 specimen No.5 had a lowest thickness reduction of 0.1 mm, and the larger weld factor of ≥ 0.8 for BGM2 specimens No.2 to No.7 had a lower thickness reduction of 0.1 mm compared to specimens No.8 to No.11 at which the thickness reduction was 0.2 mm. Meanwhile, the break location of BGM weld was not clearly affected by the weld factor if it was between 0.8 and 0.9 for those two BGMs examined herein.

3.2. Constant tensile load testing

The rupture of BGM seams subjected to a sustained tensile loading for both BGM1 and BGM2 at constant room temperature of 22 °C all occurred at the seam even though in the short-term tensile shear strength testing some failures in the sheet. This illustrates that although the tensile shear testing provides immediate insight into the bond strength within the seam and seam quality, the constant tensile load testing may offer a better indication of the long-term seam strength. Time to rupture for the acceptable welds ranged notably from 0.03 day to 29 days for BGM1 and from 0.01 day to 48 days for BGM2 when the sustained tensile load decreased from 10 kN/m (45.9% and 51.4% of sheet MTS for BGM1 and BGM2, respectively) to 1 kN/m (4.6% and 5.1% of sheet MTS for BGM1 and BGM2, respectively; Table 3), representing the prominent role of tensile load in the creep behaviour of BGM seam. Meanwhile, with a similar tensile load, the time to rupture for those two products was similar (Fig. 4). For example, time to rupture was 0.21–0.24 day for BGM1 and 0.17 day for BGM2 when the tensile load was 6 kN/m, it increased to 0.85 day for BGM1 and 0.76 day for BGM2 when the tensile load was 4 kN/m, and the time to rupture further increased to 4–5 days for BGM1 and 4.1 days for BGM2 when the tensile load reduced to 2 kN/m. The data presented herein and data published by Francey and Rowe (2024) for BGM1 correlated well (Fig. 4), showing a good repeatability of the results.

Normalizing the sustained tensile load by the MTS in the cross-machine direction, the time to rupture for BGM1 and BGM2 with acceptable welds (i.e., weld factor ≥ 0.8) was well-correlated (Fig. 4) and could be described by the equation:

$$\frac{T}{T_{MTS}} = 0.1611 \times t_{NF}^{-0.285} \tag{1}$$

Table 2
Tensile shear strength test results of BGM weld at constant room temperature of 22 °C in accordance with ASTM D7056.

BGM type	Specimen No.	Thickness reduction (mm)	Peak seam strength (kN/m)	Weld factor	Break location	GTX engagement
BGM1	1	0.1	17.4	0.80	seam	No
	2	0.5	18.2	0.83	sheet	
	3	0.3	18.0	0.83	sheet	
	4	0.1	18.6	0.85	sheet	
	5	0.1	19.1	0.88	seam	
BGM2	1	0.1	15.2	0.78	seam	No
	2	0.1	17.2	0.88		
	3	0.1	15.5	0.80		
	4	0.1	17.1	0.88		
	5	0.1	17.0	0.87		
	6	0.1	16.1	0.83		
	7	0.1	17.4	0.89		
BGM2	8 ^a	0.2	14.3	0.73	seam	No
	9 ^a	0.2	15.3	0.79		
	10 ^a	0.2	14.5	0.74		
	11 ^a	0.2	14.3	0.73		

Note.

^a Specimens were obtained from the same seamed panel.

Table 3
Summary of constant tensile load tests at a constant room temperature of 22 °C.

Load (kN/m)	BGM1 (acceptable weld) Weld factor 0.84 ± 0.03^d			BGM2 (acceptable weld) Weld factor 0.85 ± 0.05^d			BGM2 (unacceptable weld) Weld factor 0.75 ± 0.02^d		
	% of sheet MTS ^a	Time to rupture (days)	Strain at rupture (%)	% of sheet MTS ^a	Time to rupture (days)	Strain at rupture (%)	% of sheet MTS ^a	Time to rupture (days)	Strain at rupture (%)
10	45.9	0.03	30	51.4	0.01, 0.01 ^b	26, 22 ^b			
8	36.7	0.09	22	41.1	0.03, 0.04 ^b	23	41.1	0.01	16
6	27.5	0.24, 0.21 ^b	14, 13 ^b	30.8	0.17	14	30.8	0.14	16
4	18.3	0.85	- ^c	20.5	0.76	13	20.5	0.22	10
2	9.2	5.08, 4.04 ^b	7, 6.7 ^b	10.3	4.1	6.7	10.3	1.09	4
1	4.6	29	4.1	5.1	48	4.8			

Notes:
^a “MTS” represents maximum tensile strength at cross-machine direction.
^b Replicate tests.
^c Data lost due to the machine glitch.
^d Mean ± standard deviation.

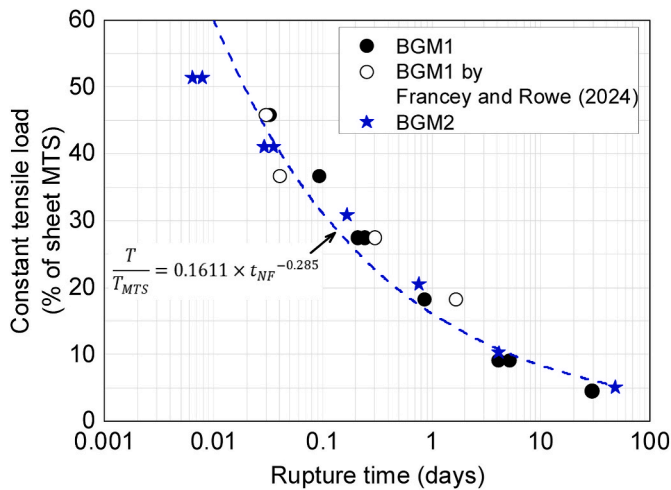


Fig. 4. Constant tensile load test results for BGM seams with weld factor ≥ 0.8 showing a fitted power function is applicable for the case without geotextile engagement. (Notes: “MTS” represents maximum tensile strength at the cross-machine direction; results were obtained at constant room temperature of 22 °C).

or inverted as:

$$t_{NF} = 0.00165 \times \left(\frac{T}{T_{MTS}} \right)^{-3.51} \quad [2]$$

where T is the sustained tensile load; T_{MTS} is the maximum tensile strength (MTS) at cross-machine direction; t_{NF} is the time to rupture in days. Given that BGM seams rely on the bitumen within the overlap to provide tensile strength if geotextiles were not engaged (Fig. 5), the good correlation among those specimens from different BGMs in Fig. 4 was hypothesized to be caused by the similar viscoelastic nature of bitumen in BGM1 and BGM2, even though the products were from different manufacturers.

At 30% of the tensile strength (analogous to 30% of yield strength at which stress crack tests are performed on the HDPE GMB), the BGM seams failed in 0.1 days (about 2 h at 22 °C compared to a minimum of 500 h required for a stress crack test at 50 °C; Fig. 4). Thus, while a BGM does not stress crack, its seams fail about more than 250 times faster than an HDPE geomembrane which stress cracks with a notch under a sustained load of 30% of its strength.

The strain at rupture, denoted as ϵ , was calculated using the cross-head extension at the initiation of seam rupture divided by the initial grip-to-grip separation of 300 mm. Strains at rupture for both BGM1 and BGM2 seamed specimens decreased with the decreasing sustained tensile load, and were generally correlated well among those different BGMs with acceptable welds (Table 3 and Fig. 6) due to the similar viscoelastic nature of bitumen. For example, strain at rupture was between 20 and 30% when the percentage of sheet MTS varied from 40 to 50%, which dropped to 4–5% when the percentage of sheet MTS was

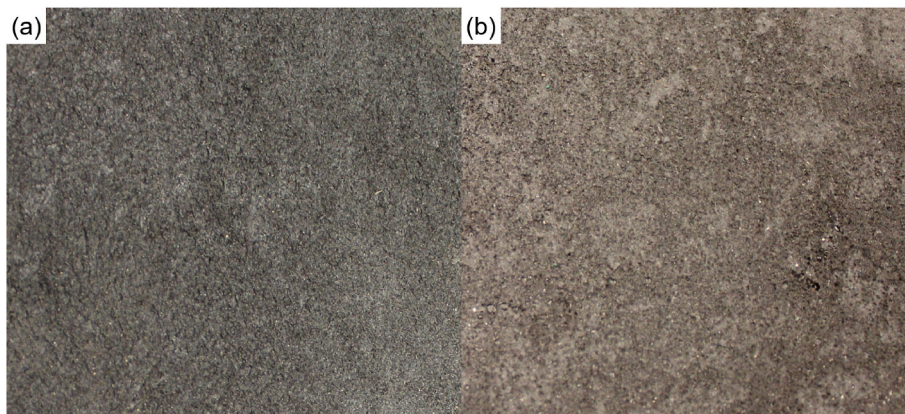


Fig. 5. Constant tensile load testing specimens at the same load of 2 kN/m after rupture showing no geotextile engagement with the weld factor between 0.8 and 0.9 for (a) BGM1 with 4-day time of rupture and (b) BGM2 with 4.1-day time of rupture.

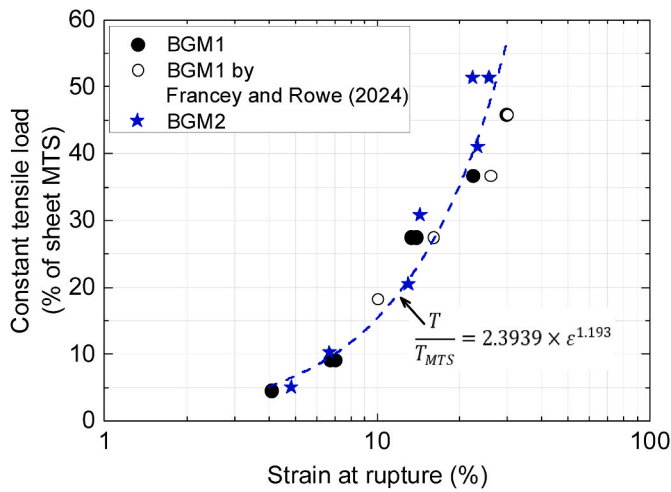


Fig. 6. Constant tensile load test results for BGM seams with weld factor ≥ 0.8 showing the correlation between the tensile load and strain at rupture for the case without geotextile engagement. (Notes: “MTS” represents maximum tensile strength at the cross-machine direction; results were obtained at constant room temperature of 22 °C).

around 5%. Thus, creep failure arising from low sustained tensile load exhibited less tensile strain, while creep failure arising from high sustained tensile load showed more ductility. Summarizing the data obtained in Table 3 and the data published by Francey and Rowe (2024), data in Fig. 6 could be correlated as:

$$\frac{T}{T_{MTS}} = 2.3939 \times e^{1.193 \epsilon} \quad [3]$$

or inverted as

$$\epsilon = 0.481 \times \left(\frac{T}{T_{MTS}} \right)^{0.838} \quad [4]$$

where ϵ is the strain at rupture.

Specimens investigating the effect of weld quality on the creep behavior of BGM seams (Table 3) were obtained from the same corresponding seamed panels as presented in Table 2. Time to rupture and strain at rupture were both notably influenced by the weld quality. For example, decreasing the sustained load from 8 kN/m, 6 kN/m, 4 kN/m, and finally to 2 kN/m, time to rupture was accordingly to be 0.03–0.04 day, 0.17 day, 0.76 day, 4.1 days for acceptable welds (weld factor ≥ 0.8), and was to be 0.01 day, 0.14 day, 0.22 day, 1.1 days for those unacceptable welds (weld factor < 0.8 ; Table 3 and Fig. 7a). Thus, the creep rupture of unacceptable welds was more easily to occur in the field. Meanwhile, strain at rupture was generally shortened for the unacceptable welds, e.g., strain at rupture dropped from 23% to 6.7% for the acceptable welds and from 16% to 4% for the unacceptable welds when reducing the sustained load from 8 kN/m to 2 kN/m (Table 3 and Fig. 7b). Therefore, unacceptable welds (weld factor < 0.8) with less bitumen involved in the bounding strength within the seamed overlap exhibited less tensile strain and faster creep failure than the acceptable welds (weld factor ≥ 0.8).

The quality of GMB welds is notably affected by welding temperature, welding speed, welding pressure and on-site conditions (Scheirs 2009). Post-failure observation of the ruptured creep specimens shows that the unacceptable weld quality of BGM2 seam was caused by the entrapment of foreign materials (e.g., debris like petiole and leaf, see Fig. 8) within the overlap during the seaming process. Those entrapped materials affected the involvement of bitumen in the overlap and the consequent integrity of BGM seam. Different from the commonly used polymeric GMB welding methods (e.g., wedge welding and extrusion welding), the top BGM panel was lifted while heating the overlap,

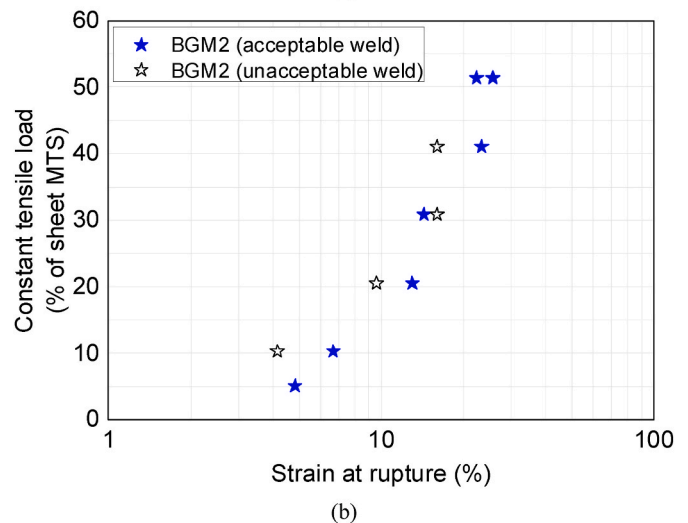
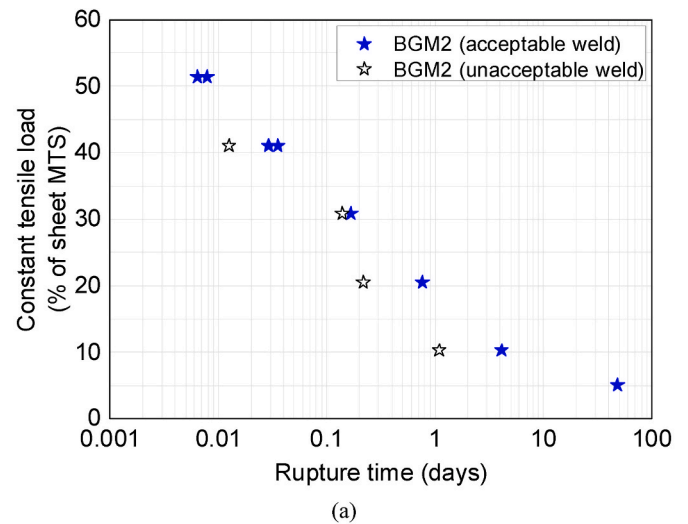


Fig. 7. Comparison of constant tensile load test results between acceptable (i.e., weld factor ≥ 0.8) and unacceptable (i.e., weld factor < 0.8) welds showing the effect of weld quality on the creep failure of BGM weld for (a) rupture time and (b) strain at rupture (Notes: “MTS” represents maximum tensile strength at the cross-machine direction; results were obtained at constant room temperature of 22 °C).

leaving a relatively large opening gap between the top and bottom panels. Thus, foreign materials were easily entrapped by the melted sticky bitumen on a windy day right before closing the overlap.

For those acceptable welds meeting the typical requirement of 0.8 weld factor based on manufacturer guidelines, creep failure arose within a very short time period (e.g., less than 48 days) relative to the designed service life of a containment facility even when the sustained tensile load exerted on the weld was as small as 5% of sheet MTS (e.g., 1 kN/m examined herein). Seams are known to be locations where stresses concentrate to a level that can be three times greater than in the sheet away from the seams (Giroud 2005; Kavazanjian et al., 2017). Thus, the long-term creep rupture of the BGM seam is a critical problem affecting the integrity of the BGM liner system. Meanwhile, the weld quality is very prone to be undermined by the on-site conditions (e.g., dust, dirt, debris, and other foreign materials) due to the sticky nature of melted bitumen and the large opening gap between the top and bottom panels during the seaming process. Therefore, as the critical location affecting the integrity of the barrier system, BGM panels are suggested to be seamed with stricter construction quality control rather than the commonly recommended trained local labor.

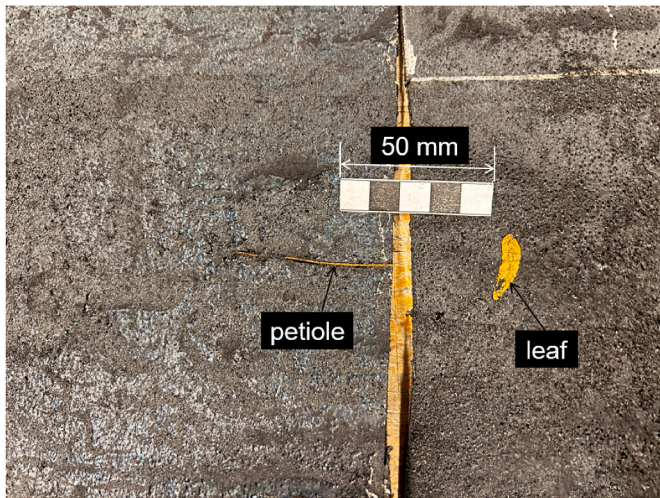
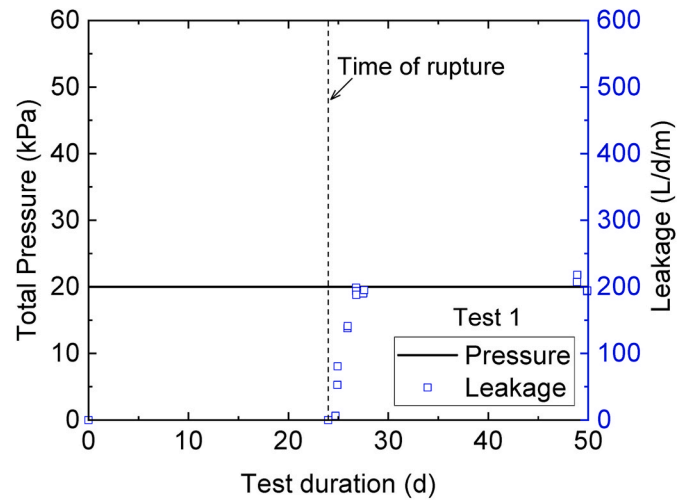


Fig. 8. Photo showing the potential field welding related problem that affected the integrity of BGM seam for the unacceptable BGM2 welds (Notes: foreign materials like debris were easily entrapped within the seam after heating and right before closing the overlap on a windy day; specimens presented here were two panels originated from different constant tensile load testing specimens).

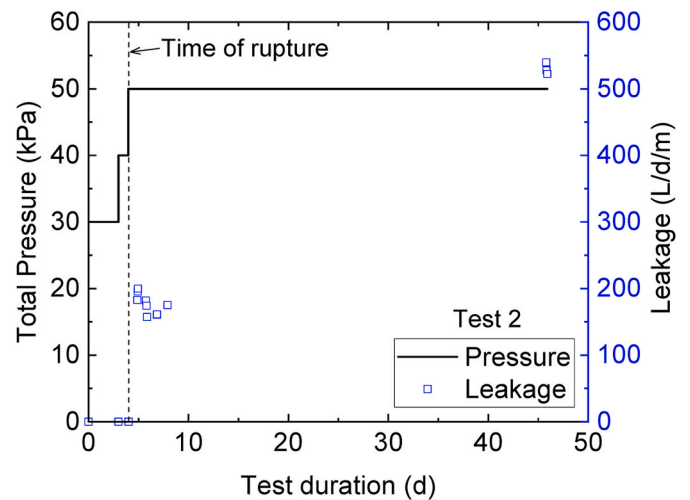
3.3. Geosynthetic liner longevity/leakage simulator testing

At a constant stress of 20 kPa above the BGM1, the seam ruptured after 24 days of testing in Test 1 (Fig. 9a). Both BGM1 in Test 2 and BGM2 in Test 3 retained their integrities after progressively staging the overlying stress from 30 kPa (3-day duration) to 40 kPa (1-day duration), while the rupture occurred readily once the stress reached 50 kPa. For example, BGM1 in Test 2 reached the failure after 0.04 day loading at 50 kPa and BGM2 in Test 3 reached the failure after 0.2 day loading at 50 kPa (Fig. 9b and c). The large-scale GLLS test results further proved the small-scale test results (i.e., constant tensile load testing) that time to rupture of BGM seam was notably affected by the sustained tensile load exerted on the weld (Table 3, Fig. 4); meanwhile, the time to rupture under the simulated field conditions in Test 2 (BGM1) and Test 3 (BGM2) generally correlated well between those two different products due to the similar viscoelastic nature of bitumen, as elaborated by the small-scale test results (Table 3, Fig. 4).

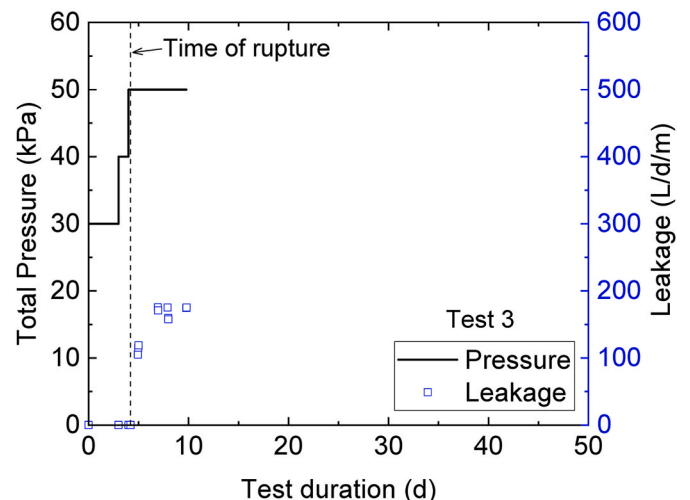
Post-test observation shows that BGM deformed downwards to the trench (Fig. 10), the greatest settlement of around 40–50 mm occurred right at the center of the trench. There was a notable slip along the top and bottom panels in the seam region. For a BGM liner resting on a rectangular trench overlain by a uniformly distributed load, the maximum tensile stress on the BGM was in the center of the long edge (Maddux et al., 1969). Thus, the rupture of the seam was considered to be initiated at the midpoint above the trench and progressively propagated towards the short edge of the trench. This is the reason that the greatest slip distance along the top and bottom panels arose in the middle of the seam above the trench (Fig. 10). For Test 2 with a 42-day loading duration at 50 kPa, the BGM seam above the trench was completely opened both on the upper sanded side and bottom PE film side, i.e., rupture length was 600 mm along the trench (Fig. 11c and d); whereas for Test 3 with a 6-day loading duration at 50 kPa, the rupture length was 400 mm on the sanded side and was 500 mm on the PE film side (Fig. 11e and f) due to a shorter test duration relative to Test 2. The 400-mm-rupture-length on the sanded side (Fig. 11e) for Test 3 was in the middle of the trench, further confirming that the rupture of the seam was initiated at the midpoint above the trench. For Test 1 with a 50-day loading duration at 20 kPa, the rupture length was 500 mm both on the sanded side and the PE film side (Fig. 11a and b) due to a smaller overburden pressure relative to Test 2. Thus, the rupture length of BGM seam was wider with a greater overburden pressure and a longer loading



(a) BGM1 in GLLS Test 1



(b) BGM1 in GLLS Test 2



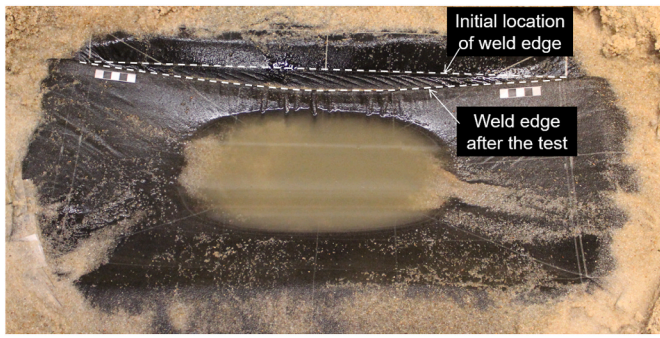


Fig. 10. Post-test observation of the BGM seam above the trench after removing the overlying materials (Note: the greater slip of weld in the middle of trench illustrates the location of the initial rupture).

duration until reaching a complete opening along the trench.

This illustrates that the rupture propagated much faster for Test 2 and Test 3 at which leakage through the ruptured seam, normalized by the water head of 1.2 m above the BGM, was 6 L/d/m-head for Test 1, 190 L/d/m-head for Test 2, and 120 L/d/m-head for Test 3 0.8-day after rupture (Table 4). The overburden stress was 50 kPa relative to that for Test 1 at which the overburden stress was 20 kPa. Leakage for Test 1 increased rapidly from 6 L/d/m at 0.8-days after rupture to 80 L/d/m at 1-day after rupture, 140 L/d/m-head at 2-day after rupture, 200 L/d/m-head at 3-day after rupture, and remained a steady leakage of 200 L/d/m-head thereafter (Fig. 9a), representing the progressively wider opening of the BGM seam under the sustained overlying stress within the first 3-day rupture, and the rupture length generally remained unchanged thereafter. Leakage for Test 1 and Test 3 before test termination

was close (i.e., 200 L/d/m-head for Test 1 vs 170 L/d/m-head for Test 3; see Fig. 9a and c) due to a similar rupture length of the BGM seam (i.e., 500 mm on both the sanded and PE film sides for Test 1 vs 400 mm on the sanded side and 500 mm on the PE film side for Test 2; see Fig. 11a, b, 11e, 11f). The largest leakage before test termination was observed at 540 L/d/m-head for Test 2 (Fig. 9b) after less than 50 days test duration due to a complete rupture along the trench (Fig. 11c and d). With a longer test duration for Test 1 and Test 3, a complete rupture along the trench could also be expected. Thus, once the rupture of BGM seam was initiated, the propagation of rupture was much faster relative to the expected service life of the BGM liner, which would eventually result in a complete failure along the uneven underlying material, regardless of the magnitude of the overlying stress.

When the BGM is used as a cover material for waste facilities, the overlying stress above the BGM is generally close to 20 kPa. In most cases, differential settlements of BGM arise from density variations and degradation or consolidation of the waste underlying material. In cold regions, thawing of near surface waste and soil placed when frozen can also lead to differential settlements of BGM. When the differential settlements arise in the seamed region, rupture of the BGM seam would occur rapidly (e.g., ≤ 24 days for GLLS test herein) and propagate along the differential settlement (Fig. 11), which eventually results in the loss of its function as a gas and fluid barrier. Increasing the stress above the BGM (e.g., when it is used as a bottom liner), the rupture of BGM seam occurs more rapidly. Therefore, the BGM is not recommended as a cover liner above waste or other material likely to experience differential settlement, and whenever it is used as a bottom barrier system, subgrade soil needs to be well-compacted to avoid imperfections (e.g., protrusions, ruts, differential settlements).

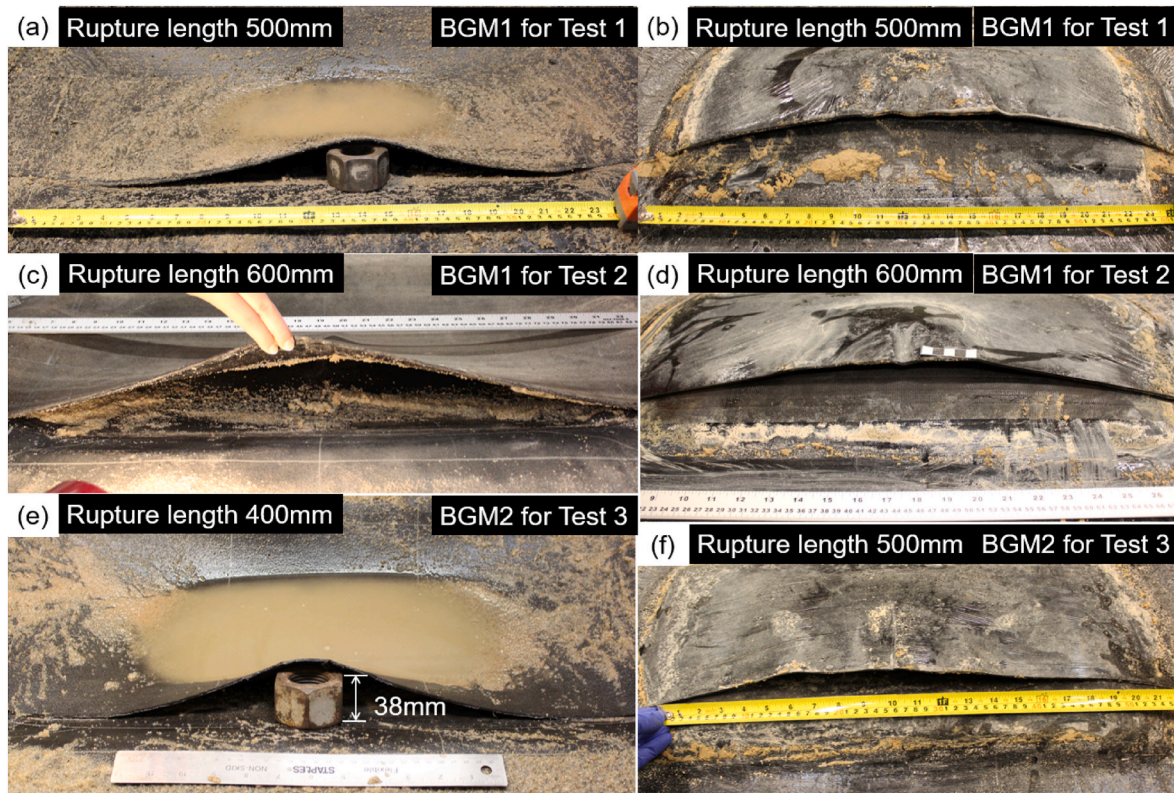


Fig. 11. Post-test observation of the BGM defective seam after applying the vertical stress for: (a) sanded side of BGM1 for Test 1 with a rupture length of 500 mm along the trench; (b) PE film side of BGM1 for Test 1 with a rupture length of 500 mm along the trench; (c) sanded side of BGM1 for Test 2 with a complete opening along the trench; (d) PE film side of BGM1 for Test 2 with a complete opening along the trench; (e) sanded side of BGM2 for Test 3 with a rupture length of 400 mm along the trench; and (f) PE film side of BGM2 for Test 3 with a rupture length of 500 mm along the trench (Notes: for Test 1, test was terminated after 50-day test duration at 20 kPa; for Test 2, test was terminated after 42-day test duration at 50 kPa; For Test 3, test was terminated after 6-day test duration at 50 kPa).

Table 4
Loading conditions and test results of geosynthetic liner longevity/leakage simulator (GLLS) testing.

Stage	Total pressure above BGM (kPa) ^b		Duration of each loading stage (days)		Loading stage duration until the rupture (days)			Leakage (L/d/m ²) through BGM weld after 0.8-day rupture		
	Test 1	Tests 2&3	Test 1	Tests 2&3	Test 1 (BGM1)	Test 2 (BGM1)	Test 3 (BGM2)	Test 1 (BGM1)	Test 2 (BGM1)	Test 3 (BGM2)
1	20	30	50	3	24	–	–	6 ^c	–	–
2	–	40	–	1	–	–	–	–	–	–
3	–	50	–	42 & 6	–	0.04	0.2	–	190 ^d	120 ^e

Notes.

- ^a Liters per day per meter water head above the BGM, measured at the water head of 1.2 m above the BGM.
- ^b Pore pressure above the BGM before rupture was 12 kPa at Stage 1, 16 kPa at Stage 2 and 19 kPa at Stage 3.
- ^c Test 1 began leaking at about 6 L/m/day and increased with time until creeping to about 200 L/d/m before terminating the test (Fig. 9a).
- ^d Test 2 began leaking at about 190 L/d/m and increased with time until creeping to about 540 L/d/m (Fig. 9b).
- ^e Test 3 began leaking at about 120 L/d/m and increased with time until creeping to about 170 L/d/m (Fig. 9c).

4. Discussions and practical implications

The creep behaviour of BGM specimens examined herein relied on the bounding of bitumen within the overlap to provide tensile strength. With more heating applied and greater seaming stress forcing the softened bitumen together during the seaming process, the reinforcement geotextiles within the core of the top and bottom BGM panels would potentially be tacked to each other. This would provide extra bounding and consequently resulted in a longer time to rupture and greater strain at rupture when the weld experienced sustained tensile load (Francey and Rowe 2024). For example, when the geotextiles were engaged in the seam, time to rupture was 4.6 days, 1.6 days, and 0.6 day with the corresponding percentage of sheet MTS of 27.5%, 36.7%, and 46%, which was notably greater than the corresponding time to rupture of 0.3 day, 0.04 day, and 0.03 day when the geotextiles were not engaged in the seam (Francey and Rowe 2024). With low or moderate heating during the seaming process, the melted bitumen only extended into a shallow depth and none of the bitumen near the geotextile was affected, as in the cases examined herein. The consequent lack of geotextile engagement resulted in lower seam tensile strength relative to the seam with geotextile engagement. However, following greater heating time and seaming stress, a higher degree of thickness reduction and excessive bitumen loss may arise, this would reduce the tensile performance of the seam as there is less bitumen engaging the geotextile core. Thus, to ensure the quality of BGM seam, the heating time and seaming stress should be given careful attention during the seaming process; this is not likely to consistently happen with a torch and a roller. Rather it would require a welding machine and a skilled welder just as for HDPE seams.

BGM seams should be assessed based on both the immediate short-term tensile strength and the likely long-term creep behavior due to the viscoelastic nature of bitumen. The research presented herein shows that although the short-term tensile shear testing can provide an immediate indication of bonding strength, constant tensile load testing and large-scale GLLS testing under the simulated field conditions may provide a better indication of seam tensile strength with time, especially for the BGM seam that is very susceptible to long-term tensile loads perpendicular to the seam direction. In the field, special care and attention should be paid to avoid placing BGMs in areas suspected to be uneven (e.g., subgrade imperfections like ruts or protrusions) or to experience significant differential settlement perpendicular to the seam direction (e.g., the variation in the stiffness of liner bedding materials).

The research conducted herein was at a constant room temperature of 22 °C. The barrier system may be exposed to elevated temperatures in both the municipal solid waste landfill and mining applications. For example, temperatures up to 40–60 °C were detected at the base of landfills where a notable leachate mound arose (Rowe 2005). Bitumen is a temperature-sensitive material. Immersion test results show that the degradation of elastomeric BGMs was accelerated by the elevated temperature (Samea and Abdelaal 2023). The impact of the temperature on the creep rupture behaviour of elastomeric bituminous geomembrane

seams is unknown but it is hypothesized that the time to failure will reduce at higher temperatures; this hypothesis needs to be tested for applications where the BGM is to be used at elevated temperatures.

5. Summary and conclusions

Small-scale tests (i.e., tensile shear strength tests, constant tensile load tests) and large-scale tests (i.e., geosynthetic liner longevity/leakage simulator (GLLS) experiments) were conducted at a constant temperature of 22 °C to evaluate the short-term and longer-term performances of BGM seams welded by a field torch. Two BGM products from different manufacturers were examined. The sustained tensile load applied for the constant tensile load testing varied from 1 kN/m (4–5% sheet maximum tensile strength) to 10 kN/m (45–51% sheet maximum tensile strength), and strains as low as 4–5%. The sustained overlying stress above the BGM for the GLLS test under the simulated field conditions varied from 20 kPa to 50 kPa. The influence of weld quality arising from the seaming process was also investigated. For the specific conditions and materials examined, the following conclusions were reached.

1. The short-term tensile shear strength testing did not provide a good indication of the long-term tensile strength of BGM seam.
2. “Good” BGM seams (weld strength/short-term sheet strength ≥0.8) were very susceptible to rupture under sustained tensile load in both small-scale and large-scale testing.
3. The creep to rupture of “good” welds was primarily affected by the viscoelastic nature of bitumen. At room temperature, the time to rupture, t_{NF} , of a “good” BGM seam was given by the relationship:

$$(T/T_{MTS}) = 0.161 t_{NF}^{0.285} \text{ or } t_{NF} \sim 0.00165 * \exp(-3.5 \ln(T/T_{MTS}))$$

With the increasing sustained tensile load from 5%, 10%, 20%, 30%, 40% of sheet maximum tensile strength, time to rupture dropped accordingly from 30–50 days, 5 days, 0.8 days, 0.2 days, and finally to 0.03 days at room temperature.

4. With a tensile load from 5% to 40% of the sheet’s maximum tensile strength, the strain at rupture increased from 4% to ~23%.
5. At 30% of the tensile strength (analogous to 30% of yield strength at which stress crack tests are performed on HDPE GMB), the BGM seams failed in 0.1 days (about 2 h at 22 °C compared to a minimum of 500 h required for a stress crack test at 50 °C). Thus, while a BGM does not stress crack, its seams fail more than 250 times faster than an HDPE geomembrane which stress cracks with a notch under a sustained load of 30% of its strength.
6. Foreign materials can be easily entrapped within the overlap by the melted sticky bitumen during welding on a windy day resulting in a “poor” weld (weld strength/short-term sheet strength <0.8). Poor

welds exhibited a faster creep failure and less tensile strain at failure than good welds.

7. Large-scale tests simulating the field conditions illustrated that the creep failure of BGM seam was notably affected by the overlying pressure. At room temperature, rupture of BGM seam occurred within 24 days at an applied stress of 20 kPa and less than 0.2 days at 50 kPa. Once initiated, rupture propagated quickly. Leakages of 170–540 L/d/m-head were observed at the end of the tests. These leakages may be acceptable in potable water reservoirs and canals but are likely to have a negative impact in containment applications. Designers need to be sensitive to potential environmental impacts and liabilities of leakage of this magnitude.

Each type of GMB has its strengths and weaknesses. BGM indeed has many advantages relative to polymeric GMBs. However, the seaming process of BGM easily attracts foreign materials inside the overlap, undermining seam integrity. Also, the creep failure of BGM seam arose within a very short period (e.g., less than 50 days) relative to the designed service life of a containment facility even when the sustained tensile load exerted on the weld was as small as 5% of sheet MTS (e.g., 1 kN/m examined herein). Large-scale tests simulating field conditions show that creep failure was likely to occur within 24 days at the overburden pressure of 20 kPa. Thus, considerable caution is required if a BGM is being considered as a cover material for waste facilities if an uneven surface or differential settlement of the underlying waste, triggered by waste degradation, consolidation, or thawing of frozen waste, are likely to occur. Also, if the BGM is being considered as a bottom liner in a containment facility, special attention is needed to avoid subgrade imperfections (e.g., ruts or protrusions).

Data

Some or all data used are available from the corresponding author by request.

CRediT authorship contribution statement

Jiyang Fan: Writing – original draft, Methodology, Investigation, Formal analysis, Data curation, Conceptualization. **R. Kerry Rowe:** Writing – review & editing, Validation, Supervision, Resources, Project administration, Methodology, Investigation, Funding acquisition, Formal analysis, Data curation, Conceptualization.

Declaration of competing interest

The authors declare there are no competing interests.

Data availability

Data will be made available on request.

Acknowledgements

The research reported in this paper was supported by the Natural Sciences and Engineering Research Council of Canada (NSERC) under Grant RGPIN-2022-03928 to RK Rowe.

References

Addis, P., Andruchow, B., Wislesky, L., 2016. Bituminous geomembrane failure as a Co-Disposal tailings storage facility. In: Proc. Tailings and Mine Waste, Banff, AB, Canada.

Chang, J.Y., Feng, S.J., Zheng, Q.T., Shen, Y., 2021. Cyclic shear behavior of GMB/GCL composite liner. *Geotext. Geomembranes* 49 (3), 593–603.

Cheng, Q., Tang, C.S., Zeng, H., Zhu, C., An, N., Shi, B., 2020. Effects of microstructure on desiccation cracking of a compacted soil. *Eng. Geol.* 265, 105418.

Ewais, A.M.R., Rowe, R.K., Brachman, R.W.I., Arneppalli, D.N., 2014. Service life of a high-density polyethylene geomembrane under simulated landfill conditions at 85° C. *J. Geotech. Geoenviron. Eng.* 140 (11), 04014060.

Fan, J.Y., Rowe, R.K., 2022a. Seepage through a circular geomembrane hole when covered by fine-grained tailings under filter incompatible conditions. *Can. Geotech. J.* 59 (3), 410–423.

Fan, J.Y., Rowe, R.K., 2022b. Piping of silty sand tailings through a circular geomembrane hole. *Geotext. Geomembranes* 50 (1), 183–196.

Fan, J.Y., Rowe, R.K., 2023a. Effect of subgrade on leakage through a defective geomembrane seam below saturated tailing. *Geotext. Geomembranes* 51 (2), 360–369.

Fan, J.Y., Rowe, R.K., 2023b. Effect of geosynthetic component characteristics on the potential for GCL internal erosion. *Geotext. Geomembranes* 51 (4), 85–94.

Fan, J.Y., Rowe, R.K., 2023c. Effect of subgrade on tensile strains in a geomembrane for tailings storage applications. *Can. Geotech. J.* 60 (1), 18–30.

Fan, J.Y., Rowe, R.K., 2023d. Leakage through a circular geomembrane hole overlain and underlain by silty sand tailings. *Geosynth. Int.* 1–12. <https://doi.org/10.1680/jgein.23.00028>.

Fan, J.Y., Rowe, R.K., 2024a. Effect of a lateral drainage layer on leakage through a defect in a geomembrane overlain by saturated tailings. *Geotext. Geomembranes* 52 (4), 383–395.

Fan, J.Y., Rowe, R.K., 2024b. Effect of a soluble subgrade on leakage through a geomembrane defect. *Geosynth. Int.* 31 (3), 314–326.

Francey, W., Rowe, R.K., 2024. Factors affecting the tensile strength of bituminous geomembrane seams. *Geosynth. Int.* (in press).

Giroud, J.P., 2005. Quantification of geosynthetic behavior. *Geosynth. Int.* 12 (1), 2–27.

Giroud, J.P., Bonaparte, R., 1989a. Leakage through liners constructed with geomembranes—part I. Geomembrane liners. *Geotext. Geomembranes* 8 (1), 27–67.

Giroud, J.P., Bonaparte, R., 1989b. Leakage through liners constructed with geomembranes—Part II. Composite liners. *Geotext. Geomembranes* 8 (2), 71–111.

Giroud, J.P., Tisseau, B., Soderman, K.L., Beech, J.F., 1995. Analysis of strain concentration next to geomembrane seams. *Geosynth. Int.* 2 (6), 1049–1097.

Kavazanjian, E., Andresen, J., Gutierrez, A., 2017. Experimental evaluation of HDPE geomembrane seam strain concentrations. *Geosynth. Int.* 24 (4), 333–342.

Maddux, G.E., Vorst, L.A., Giessler, F.J., Moritz, T., 1969. *Stress Analysis Manual*. Dayton: Technology Incorporated.

Ng, C.W.W., Guo, H., Ni, J., Zhang, Q., Chen, R., Zhang, Y., 2023. Effects of plant-biochar interaction on the performance of a landfill cover system: field monitoring and numerical modelling. *Can. Geotech. J.* 60 (11), 1663–1680.

Peggs, L., 2008. Prefabricated bituminous geomembrane: a candidate for exposed geomembrane caps for landfill closures. In: Proceedings of the First Pan American Geosynthetics Conference and Exhibition, Cancun, Mexico, Industrial Fabrics Association International (IFAI), USA, pp. 191–197.

Peggs, L.D., Gassner, F., Scheirs, J., Tan, D., Arango, A.M.N., Burkard, B., 2014. Is there a resurgence of stress cracking in HDPE geomembranes. In: Proceedings 10th International Geosynthetics Conference, Berlin, Germany, DGGT, Essen, Germany (CD-ROM).

Pu, H., Qiu, J., Zhang, R., Zheng, J., 2018. Assessment of consolidation-induced VOC transport for a GML/GCL/CCL composite liner system. *Geotext. Geomembranes* 46 (4), 455–469.

Rollin, A.L., Marcotte, M., Jacqueline, T., Chaput, L., 1999. Leak location in exposed geomembrane liners using an electrical leak detection technique. In: Proceedings of Geosynthetic'99, Industrial Fabrics Association International, Boston, USA, IFAI, Roseville, MI, USA, vol. 2, pp. 615–626.

Rowe, R.K., 1998. Geosynthetics and the minimization of contaminant migration through barrier systems beneath solid waste. In: Proceedings 6th International Conference on Geosynthetics, Atlanta, vol. 1, pp. 27–103.

Rowe, R.K., 2005. Long-term performance of contaminant barrier systems. *Geotechnique* 55 (9), 631–678.

Rowe, R.K., 2012. Short and long-term leakage through composite liners. *Can. Geotech. J.* 49 (2), 141–169.

Rowe, R.K., 2020. Protecting the environment with geosynthetics: 53rd Karl Terzaghi lecture. *J. Geotech. Geoenviron. Eng.* 146 (9), 04020081.

Rowe, R.K., Fan, J.Y., 2021. Effect of geomembrane hole geometry on leakage overlain by saturated tailings. *Geotext. Geomembranes* 49 (6), 1506–1518.

Rowe, R.K., Fan, J.Y., 2022. A general solution for leakage through geomembrane defects overlain by saturated tailings and underlain by highly permeable subgrade. *Geotext. Geomembranes* 50 (4), 694–707.

Rowe, R.K., Fan, J., 2024. The application of geosynthetics in tailings storage facilities: a general review. *Mining* 4 (2), 447–468.

Rowe, R.K., Hosney, M.S., 2013. Laboratory investigation of GCL performance for covering arsenic contaminated mine wastes. *Geotext. Geomembranes* 39, 63–77.

Rowe, R.K., Jefferis, S., 2022. Protecting the environment from contamination with barrier systems: advances and challenges, State-of-the-Art Lecture. In: Proceedings of the 20th International Conference on Soil Mechanics and Geotechnical Engineering, Sydney, Australia, pp. 187–293.

Rowe, R.K., Shoaib, M., 2017. Long-term performance of high-density polyethylene (HDPE) geomembrane seams in municipal solid waste (MSW) leachate. *Can. Geotech. J.* 54 (12), 1623–1636.

Rowe, R.K., Yu, Y., 2019. Magnitude and significance of tensile strains in geomembrane landfill liners. *Geotext. Geomembranes* 47 (3), 439–458.

Rowe, R.K., Quigley, R.M., Brachman, R.W.I., Booker, J.R., 2004. *Barrier Systems for Waste Disposal Facilities*. Taylor & Francis, London (E & FN Spon).

Rowe, R.K., Brachman, R.W.I., Irfan, H., Smith, M.E., Thiel, R., 2013. Effect of underliner on geomembrane strains in heap leach applications. *Geotext. Geomembranes* 40, 37–47.

- Samea, A., Abdelaal, F.B., 2023. Durability of two bituminous geomembranes (BGMS) with different thicknesses in MSW synthetic leachate. *Waste Management* 165, 179–188.
- Scheirs, J., 2009. *A Guide to Polymeric Geomembranes: a Practical Approach*. John Wiley & Sons.
- Tang, C.S., Zhu, C., Cheng, Q., Zeng, H., Xu, J.J., Tian, B.G., Shi, B., 2021. Desiccation cracking of soils: a review of investigation approaches, underlying mechanisms, and influencing factors. *Earth Sci. Rev.* 216, 103586.
- Touze, N., 2020. Healing the world: a geosynthetics solution. *Geosynth. Int.* 1–31.
- Touze-Foltz, N., Farcas, F., 2017. Long-term performance and binder chemical structure evolution of elastomeric bituminous geomembranes. *Geotext. Geomembranes* 45 (2), 121–130.
- Yan, H., Wu, J., Thomas, H.R., Ding, H., Zhan, L., Xie, H., 2021. Analytical model for coupled consolidation and diffusion of organic contaminant transport in triple landfill liners. *Geotext. Geomembranes* 49 (2), 489–499.
- Zhan, L.T., Chen, C., Bouazza, A., Chen, Y.M., 2018. Evaluating leakages through GMB/GCL composite liners considering random hole distributions in wrinkle networks. *Geotext. Geomembranes* 46 (2), 131–145.
- Zhang, L., Bouazza, A., Rowe, R.K., Scheirs, J., 2017. Effect of welding parameters on properties of HDPE geomembrane seams. *Geosynth. Int.* 24 (4), 408–418.